High Entropy Perovskite Oxides (HEPOs) for Catalytic Soot combustion

Huimin Ma, Xianqiu Song, Jin Wang*, Ying Xin and Zhaoliang Zhang

University of Jinan, Jinan, Shandong 250022, China

*Corresponding author's e-mail: chm_wangjin01@ujn.edu.cn

Abstract. Catalytic soot combustion has been considered as one of the most efficient technologies for emitted soot particles. In this study, HEPO catalysts were successfully synthesised using the sol-gel method. The catalysts were analysed using XRD, N_2 adsorption and O_2-TPO. These results indicate that the synergistic effects of different elements at the B-site of high-entropy perovskite produce different soot catalytic activities. Based on atomic radius and tolerance factor effects, B-site elements such as Fe, Co, Mn, Ni and Cu produce excellent soot catalytic activities. This work provides a promising high-entropy strategy for developing of highly efficient oxide-based soot combustion catalysts.

Keywords: Diesel vehicle exhaust, Soot combustion, High Entropy Perovskite Oxide

1 Introduction

As a pollutant emitted by diesel vehicle exhaust, soot particles have caused serious damages to the environment and human health [1]. Firstly, soot particles are the main cause of severe haze weather. Conversely, soot particles can be easily inhaled by humans because of their smaller diameter and size, which seriously harms human health. Among the elimination methods of soot particles, catalytic combustion technology has attracted much attention. But this technology depends strongly on the performance of catalysts.

Up to now, many types of catalysts have been synthesized to facilitate soot oxidation, such as catalysts with ordered macroporous structures [2], supported catalysts with noble metal or alkali metal [3-5] and transition metal oxides [6]. Among these catalysts, perovskite-type (ABO_3) oxide catalysts have attracted great attention [7, 8] owing to their distinctive structure and the flexibility of the A- and B-sites. With the increase of the number of doping elements, many new characterizations appear. Such materials, composed of nearly equimolar of multiple components (five or more elements) were defined as high-entropy oxides. Most recently, high-entropy perovskite oxides (HEPOs) show excellent catalytic activity and stability in many systems of catalytic reaction. And that high entropy perovskite oxide lays a good foundation for catalytic

© The Author(s) 2025
W. He et al. (eds.), *Proceedings of the 2024 10th International Conference on Advances in Energy Resources and Environment Engineering (ICAESEE 2024)*, Atlantis Highlights in Engineering 36,
https://doi.org/10.2991/978-94-6463-708-3_4

soot combustion due to its four core effects. [9, 10, 11]. For the catalytic soot combustion, HEPOs were expected to have outstanding performance, due to their distinctive structure and unique physicochemical properties. Therefore, studies on the application of HEPOs in the catalytic elimination of soot would provide new pathway for the development of efficient catalysts. High-entropy materials are frequently employed in catalytic oxidation due to their distinctive characteristics. This paper aims to create a perovskite with B-site high-entropy by doping five metal elements. One of the effects of high-entropy materials is the cocktail effect, in which different combinations of elements will produce different catalytic properties. In this paper, we not only successfully prepared B-site high entropy perovskite catalyst, but also further screened the B-site element combination.

Herein, a series HEPOs with five metal elements assembled into $LaMnO_3$ lattice were successfully prepared. With the variations of element composition, the catalytic activity is different, and the catalyst of $La(FeCoMnNiCu)O_3$ exhibit the best performance.

2 Experimental Section

2.1 Catalyst Preparation

All the samples were synthesized by a citric acid assisted sol-gel method. Typically, All precursor nitrates were dissolved in water. Then, 5.76 g citric acid was added to the above solution. The mixture was agitated for a period of two hours at room temperature, and then transferred to a water bath (80 °C) and stirred at 300 rpm until the solution evaporated. The obtained wet gel was then transferred to an oven and dried overnight at 80 °C to obtain a sponge-like dry gel. Finally, the dry gel powder was placed in the preheated muffle furnace (350 °C) for 2 h. Next, the calcination temperature was gradually increased to 750 °C, and the sample was calcined at 750 °C for 4 h. This sample was labeled as $La(FeCoMnNiCu)O_3$. According to the molecular formula, the other three samples were synthesized with the specific amounts of metal salt precursors, and labeled as $La(FeCoMnNiCr)O_3$, $La(FeCoMnAlCr)O_3$ and $La(FeCoMnAlCu)O_3$.

2.2 Catalyst Characterization

XRD patterns were recorded on a Rigaku X-ray diffractometer using Cu Kα radiation. $2\theta = 20°$ to 80°, scanning rate $10°\cdot min–1$. BET surface areas from N_2 adsorption/desorption isotherms, Micromeritics ASAP2020M.The specific test procedure is as follows: Weigh about 100 mg of dry powder sample, degas the sample under vacuum environment at 300 ℃ for 8 h, remove the adsorbed water and impurities on the sample surface; After the degassing is completed, static adsorption analysis of pore structure is performed in liquid nitrogen environment with nitrogen as the adsorption medium. After the analysis is completed, the system automatically generates a report.

2.3 Activity Measurement

TPO reactions were carried out in the fixed bed micro-reactor using Printex-U from Degussa [12] as the model soot. The TPO was initiated at a heating rate of 5 °C·min^{-1} from room temperature to 700 °C in a gas flow of 5 vol.% O_2/He. The concentrations of produced CO and CO_2 were monitored on-line by GC (Shandong Lunan Ruihong SP-7890). Finally, the data are organized and the conversion rate curve is obtained. The temperature when the conversion rate of carbon smoke is 10%, 50% and 90% is called the characteristic temperature T_{10}, T_{50} and T_{90} respectively.

3 Results and Discussion

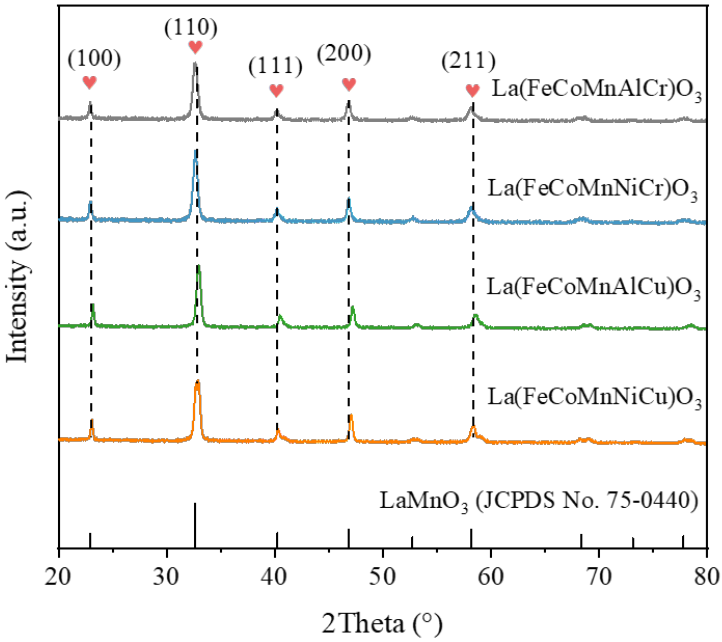

Fig. 1. XRD patterns of HEPOs catalysts.

Firstly, the configurational entropy of a series of high entropy perovskite oxides is calculated according to the configurational entropy formula. The configurational entropy of La(FeCoMnCrAl)O3, La(FeCoMnNiCr)O3, La(FeCoMnAlCu)O3 and La(FeCoMnNiCu)O3 are 1.5R. According to the definition of high entropy oxides, the prepared catalysts all conform to the concept of high entropy. The configurational entropy of the series of HEPOs is calculated according to the configurational entropy formula (1):

$$\Delta S_{config} = -R[(\sum_{i=1}^{N} xi \ln xi) + (\sum_{j=N+1}^{N+M} xj \ln xj)] \quad (1)$$

In general, a material is recognized as a high entropy material when its configurational entropy meets the requirement of $\Delta S_{config} \geq 1.5R$ [13]. Obviously, all the samples are high entropy materials according to the definition of high entropy oxides.

Furthermore, so as to investigate the crystal structure, the XRD patterns of the HEPOs series catalysts were evaluated. As shown in Figure 1, the peaks of HEPOs catalyst at 22.9, 32.6, 40.2, 46.8, 52.7, 58.2, 68.3, 73.1 and 77.8° can be indexed to (100), (110), (111), (200), (210), (211), (220), (221) and (310) lattice planes, respectively. These peaks agree well with the cubic perovskite-type $LaMnO_3$ structure (JCPDS No.75-0440), and no impurity oxide phase is observed. These results demonstrate that single phase perovskite oxides with ABO_3 type structure have been successfully prepared.

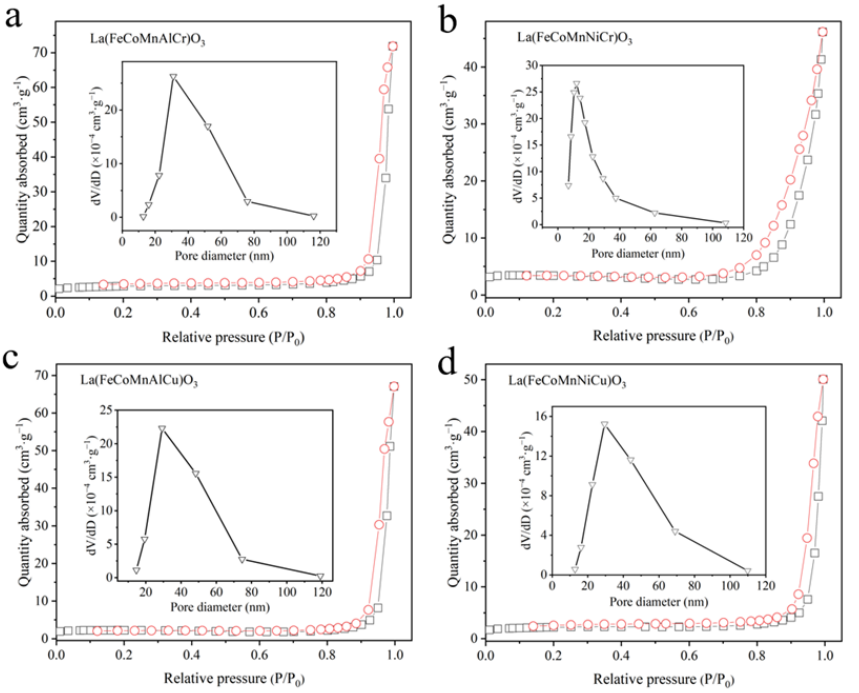

Fig. 2. N2 adsorption/desorption isotherms and pore distribution curves (inset) for (a) $La(FeCoMnAlCr)O_3$;(b) $La(FeCoMnNiCr)O_3$; (c) $La(FeCoMnAlCu)O_3$ and (d) La(FeCoMnNiCu)O_3.

Table 1. BET surface area, average pore size, and pore volume of HEPOs catalysts.

Catalysts	Surface area ($m^2 \cdot g^{-1}$)	Average pore diameter (nm)	Pore volume ($cm^3 \cdot g^{-1}$)
$La(FeCoMnAlCr)O_3$	9.8	39.6	0.11
$La(FeCoMnNiCr)O_3$	11.1	21.5	0.07
$La(FeCoMnAlCu)O_3$	8.3	40.8	0.10
$La(FeCoMnNiCu)O_3$	7.6	41.7	0.08

The surface area and pore structure affect catalysts' catalytic performance. Therefore, the BET method is used to determine the surface area and the N_2 absorption and desorption curves are used to evaluate the pore capacity. The detailed analytical data are summarized in Figure. 2 and Table 1. As shown in Figure. 2, the N_2 adsorption/desorption isotherms of a series of HEPOs show a typical IV type, where the rapid increase of N_2 adsorption in the range of 0.8–1.0 (P/P_0) indicates the existence of a certain number of the macropores. As shown in Table 1, the average pore diameter is in the range of 20 nm to 50 nm, suggesting that the main pore of the catalysts is macropore. However, the high calcination temperature for the formation of high entropy may lead to the sintering and the collapse of amount of mesopore and macropore pore structure, which result from the decomposition of citric acid during the calcination process, thereby the specific surface areas of all HEPO samples are low.

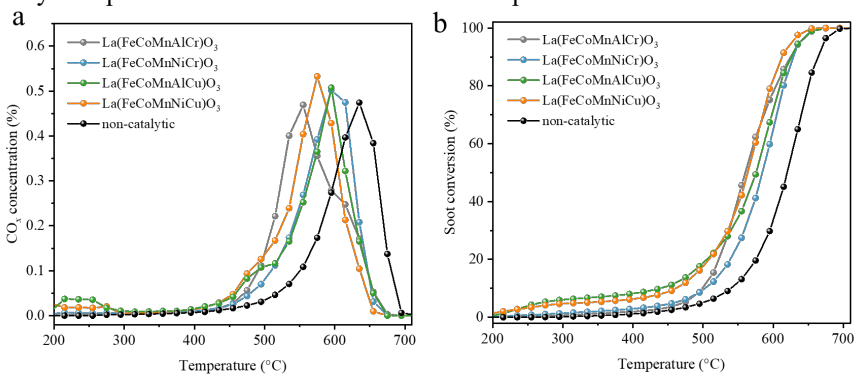

Fig. 3. Catalytic performances of HEPOs catalysts for soot combustion under the loose contact condition. (a) O_2-TPO profiles, (b) Soot conversion profiles.

Table 2. Catalytic activities of the HEPOs catalysts for soot combustion.

Samples	T_{10} (°C)	T_{50} (°C)	T_{90} (°C)	S_{CO2} (%)
soot	540	620	663	63
La(FeCoMnNiCr)O_3	504	585	629	94
La(FeCoMnAlCu)O_3	440	575	626	100
La(FeCoMnNiCu)O_3	463	560	611	99
La(FeCoMnAlCr)O_3	498	560	624	84

The properties of the prepared catalysts were tested, and the test results were shown in Figure 3 and Table 2. These results show that the HEPOs catalysts exhibit high activity during the catalytic soot combustion reaction compare to non-catalytic soot combustion, and the La(FeCoMnNiCu)O_3 exhibits the best performance. For the La(FeCoMnAlCu)O_3 sample, both the T_{50} and the T_{90} values are higher than the corresponding values of La(FeCoMnNiCu)O_3 about 15 °C, suggesting the lower activity for soot combustion. Interestingly, a significant decrease in CO_2 selectivity was observed for La(FeCoMnNiCr)O_3 (94%) and La(FeCoMnAlCr)O_3 (84%), both of which contain the element Cr doping, suggesting that the Cr doping may be detrimental to CO_2 selectivity. According to the mentioned above, it can be concluded that the HEOPs produces excellent catalytic soot combustion performance, and the catalytic activity of HEPOs

for soot combustion is significantly affected by the element composition.Among the prepared series of high-entropy perovskite catalysts, T_{50} and T_{90} of La(FeCoMnNiCu)O_3 high-entropy perovskite catalysts are the lowest. And the carbon smoke selectivity is 99%. It shows that the synergistic effect between these five elements produces excellent catalytic soot combustion performance.

4 Conclusion

A series of high entropy perovskite catalysts have been synthesized by the sol-gel method. XRD results show that all samples are single phase perovskite oxides with ABO_3 type structure. According to N_2 adsorption results, the main pore of the catalysts is macropore and has low surface area. Importantly, all the HEPOs show excellent activity for soot combustion. This work provides a good idea and basis for the research of soot catalyst.

References

1. Shao J, Lan X, Zhang C, Cao C and Yu Y. (2022) Recent advances in soot combustion catalysts with designed micro-structures. Chinese Chem. Let, 33: 1763-1773.
2. Zhang P, Mei X L, Zhao X C, Xiong J, Li Y F, Zhao Z and Wei Y C. (2021) Boosting catalytic purification of soot particles over double Perovskite-Type $La_{2-x}K_xNiCoO_6$ catalysts with an ordered macroporous structure. Environ. Sci. Technol., 55: 11245-11254.
3. Li Y F, Qin T, Wei Y C, Xiong J, Zhang P, Lai K Z, Chi H J, Liu X, Chen L W, Yu X L, Zhao Z, Li L N and Liu J. (2023) A single site ruthenium catalyst for robust soot oxidation without platinum or palladium. Nat. Commun., 14: 7149.
4. Yu D, Wang L Y, Zhang C L, Peng C, Yu X H, Fan X Q, Liu B, Li K X, Li Z G, Wei Y C, Liu J and Zhao Z. (2022) Alkali Metals and Cerium-Modified La-Co-Based Perovskite Catalysts: Facile Synthesis, Excellent Catalytic Performance, and Reaction Mechanisms for Soot Combustion. ACS Catal., 12: 15056-15075.
5. Liu T Z, Li Q, Xin Y, Zhang Z L, Tang X F, Zheng L R and Gao P-X. (2018) Quasi free K cations confined in hollandite-type tunnels for catalytic solid (catalyst)-solid (reactant) oxidation reactions. Appl. Catal., B, 232: 108-116.
6. Lin X T, Li S J, He H, Wu Z, Wu J L, Chen L M, Ye D Q and Fu M L. (2018) Evolution of oxygen vacancies in MnO_x-CeO_2 mixed oxides for soot oxidation. Appl. Catal., *B*, 223: 91-102.
7. Peng X S, Lin H, Shangguan W F and Huang Z. (2007) A highly efficient and porous catalyst for simultaneous removal of NO_x and diesel soot. Catal. Commun, 8: 157-161.
8. Zhao K, Li J M, Wang L Y, Li D, Liu B N, Li R J, Yu X H, Wei Y C, Liu J and Zhao Z. (2022) Preparation of cordierite monolith catalysts with the coating of K-Modified spinel $MnCo_2O_4$ oxide and their catalytic performances for soot combustion. *Catalysts*, 12: 295.
9. Wang H, Liu J, Zhao Z, Wei Y C and Xu C M. (2012) Comparative study of nanometric Co-, Mn- and Fe-based perovskite-type complex oxide catalysts for the simultaneous elimination of soot and NO from diesel engine exhaust. Catal. Today, 184: 288-300.
10. Nie S Y, Wu L, Zhao L C and Zhang P F. (2021) Enthalpy-change driven synthesis of high-entropy perovskite nanoparticles. Nano Res, 15: 4867.

11. Duan X L, Wang X P, Xu L, Ma T T, Shu Y, Hou S T, Niu Q and Zhang P F. (2023) Incorporating three-dimensional ordered macropores into high-entropy oxides for catalytic soot combustion. J. Mater. Chem., A, 11: 19696-19706.
12. Neeft J P A, Makkee M and Moulijn J A. (1996) Metal oxides as catalysts for the oxidation of soot. Chem. Eng. J., 64: 295-302.
13. Wang Y, Mi J X and Wu Z-S. (2022) Recent status and challenging perspective of high entropy oxides for chemical catalysis. Chem Catal, 2:1624-1656.

Open Access This chapter is licensed under the terms of the Creative Commons Attribution-NonCommercial 4.0 International License (http://creativecommons.org/licenses/by-nc/4.0/), which permits any noncommercial use, sharing, adaptation, distribution and reproduction in any medium or format, as long as you give appropriate credit to the original author(s) and the source, provide a link to the Creative Commons license and indicate if changes were made.

The images or other third party material in this chapter are included in the chapter's Creative Commons license, unless indicated otherwise in a credit line to the material. If material is not included in the chapter's Creative Commons license and your intended use is not permitted by statutory regulation or exceeds the permitted use, you will need to obtain permission directly from the copyright holder.